Letter

Possible insulator-pseudogap crossover in the attractive Hubbard model on the Lieb lattice

Kukka-Emilia Huhtinen ◉ and Päivi Törmä ◉*

Department of Applied Physics, Aalto University, 00076 Aalto, Finland

We study the attractive Hubbard model on the Lieb lattice to understand the normal state above the superconducting critical temperature in a flat band system. We use cluster dynamical mean-field theory to compute the two-particle susceptibilities with full quantum fluctuations included in the cluster. At interaction strengths lower than the hopping amplitude, we find that the normal state on the flat band shows insulating behavior stemming from the localization properties of the flat band. A flat-band enhanced pseudogap with a depleted spectral function arises at larger interactions.

Flat, dispersionless energy bands host superconductivity governed by the quantum geometry and topology of the band [1–5]. The predicted transition temperature exceeds exponentially that of conventional superconductors [6–9], promising superconductivity at elevated temperatures. The observations of superconductivity and insulating phases at quasiflat bands in twisted bilayer graphene [10–12] reinforce such prospects. The nature of the normal state above the critical temperature of a flat-band superconductor is, however, an outstanding open question. A Fermi liquid is excluded due to the absence of a Fermi surface [13]. As the band width and kinetic energy are zero, any attractive interaction could be anticipated to cause pairing already in the normal state. Indeed preformed pairs [14,15] and a pseudogap [16–18] have been suggested. Here we show that the normal state in a Lieb lattice features, for decreasing interaction, a *crossover from a flat-band enhanced pseudogap to a non-Fermi liquid with insulating properties*. For small interactions, when lowering the temperature, one could thus expect an insulator-superconductor transition unique to flat-band systems.

The mean-field superconducting order parameter vanishes at the critical temperature. Understanding the normal state is thus inherently a beyond mean-field problem. Two-particle properties, that is, four-operator correlations must be evaluated with quantum fluctuations included. For this, we use a cluster expansion of dynamical mean-field theory (DMFT) [19]. DMFT has been used previously to investigate, for example, the normal-state properties of the attractive single-band Hubbard model [20–23], and its cluster variants for studies of pairing fluctuations with different geometries [24]. The normal state of (partially or nearly) flat-band systems with repulsive interactions has also been studied in Refs. [25–29]. We calculate the orbital-resolved pair and spin susceptibilities based on two-particle Green's functions.

We focus on the Lieb lattice, shown in Fig. 1(a), due to its conceptual simplicity and experimental relevance. The localized flat-band states reside at the lattice sites A and C

only, and can be monitored separately from site B both in experiments and simulations. This gives a means of distinguishing flat-band effects. The Lieb lattice has been realized experimentally for ultracold gases [30,31], in designer lattices made by atomistic control [32,33] and in photonic lattices [34]. Some covalent-organic frameworks are also predicted to provide the Lieb lattice [35]. We relate our predictions of the insulating and pseudogap phases to generic flat-band effects to unveil their relevance beyond the Lieb lattice, for instance for moiré materials [36] where bands of different degree of flatness can be designed.

The band structure of the Lieb lattice, shown in Fig. 1(b), features two dispersive bands and a perfectly dispersionless flat band (FB),

$$E_\pm(\boldsymbol{k}) = \pm t\sqrt{2}\sqrt{2 + \cos(k_x) + \cos(k_y)}, \ E_{\mathrm{FB}} = 0, \quad (1)$$

where the indices $+$ and $-$ refer to the upper and lower dispersive band, respectively, and t is the nearest-neighbor hopping amplitude. The lattice constant is taken as $a = 1$.

We study the attractive Hubbard model with the Hamiltonian

$$H = \sum_\sigma \sum_{i\alpha,j\beta} t_{ij} c^\dagger_{\sigma,i\alpha} c_{\sigma,j\beta} - \sum_\sigma \sum_{i\alpha} \mu_\sigma n_{\sigma,i\alpha} \quad (2)$$

$$+ U \sum_{i\alpha} (n_{\uparrow,i\alpha} - 1/2)(n_{\downarrow,i\alpha} - 1/2), \quad (3)$$

where $c^\dagger_{\sigma,i\alpha}$ is the creation operator for a fermion with spin $\sigma = \uparrow, \downarrow$ in the unit cell i and the sublattice $\alpha = A, B, C$ and $n_{\sigma,i\alpha} = c^\dagger_{\sigma,i\alpha} c_{\sigma,i\alpha}$. The hopping amplitude t_{ij} is t between nearest neighbors and 0 otherwise. Below, all energies are in units of the hopping t. The on-site interaction strength is denoted by U.

To study normal-state properties, we use a cluster expansion of DMFT where we use one unit cell of the Lieb lattice as our cluster [see Fig. 1(a)]. In this method, the lattice model is mapped to an effective Anderson impurity model, and the lattice quantities are computed self-consistently. The self-energy is assumed to be uniform and local to each unit cell, $\Sigma_{ij} \approx \Sigma \delta_{ij}$. Here, Σ is a matrix in the orbital indices.
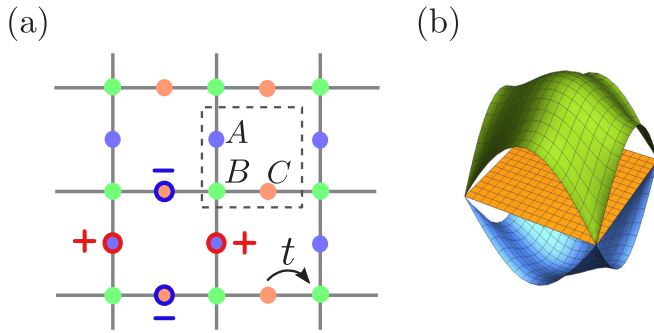
*paivi.torma@aalto.fi

FIG. 1. (a) The Lieb lattice. The unit cell indicated with dashed lines is used as a cluster in DMFT. The three sublattices are labeled A, B, and C as shown. An example of a localized FB state is shown in the lower left-hand corner. The A and C sites on a square plaquette have amplitudes of alternating sign. Since we consider only nearest-neighbor hopping, this state is localized by destructive interference. (b) Band structure of the Lieb lattice. The FB is at energy $E = 0$.

DMFT has been able to qualitatively describe topological interacting states [37,38]. Flat-band superconductivity is governed by quantum geometry and topology of the band [1–5], but its essence is in Wannier function overlap at the local level [15,39]. DMFT and mean-field predictions have been shown to agree with exact diagonalization and Quantum Monte Carlo in several attractively interacting flat-band systems [2,3,14,17,18,39].

More precisely, the principle of DMFT is as follows. The self-energy $\Sigma(i\omega_n)$ and Green's function $G(\mathbf{k}, i\omega_n)$ are related by the Dyson equation

$$G(\mathbf{k}, i\omega_n) = [G^0(\mathbf{k}, i\omega_n)^{-1} - \Sigma(i\omega_n)]^{-1}, \quad (4)$$

where $G^0(\mathbf{k}, i\omega_n)$ is the noninteracting Green's function and ω_n are fermionic Matsubara frequencies. To map the lattice model to an impurity model, we consider the local part of the Green's function $\overline{G}(i\omega_n) = \sum_{\mathbf{k}} G(i\omega_n, \mathbf{k})$. The bath Green's function of the impurity model is obtained from

$$\mathcal{G}^0(i\omega_n) = [\overline{G}^{-1}(i\omega_n) + \Sigma(i\omega_n)]^{-1}. \quad (5)$$

In this work, the impurity problem defined by $\mathcal{G}^0(i\omega_n)$ is solved using an interaction expansion continuous time Monte Carlo solver [40,41]. The solution of the impurity problem provides the impurity Green's function $\mathcal{G}(i\omega_n)$ and a new estimate for the self-energy. In DMFT, the self-energy of the impurity is equal to the self-energy of the lattice, so the result can be plugged into Eq. (4). This procedure is repeated until the self-consistency condition $\overline{G}(i\omega_n) = \mathcal{G}(i\omega_n)$ is fulfilled.

Calculation of the two-particle susceptibilities is a central and highly nontrivial part of our work. The main ideas are discussed here, and further details are given in the Supplemental Material [42]. This procedure [43] allows one to compute the generalized susceptibilities

$$\chi_{ijkl}(\tau_1, \tau_2, \tau_3) = G^{(4)}_{ijkl}(\tau_1, \tau_2, \tau_3) - G_{ij}(\tau_1, \tau_2)G_{kl}(\tau_3, 0), \quad (6)$$

where $G^{(4),\mathrm{ph}}_{ijkl}(\tau_1, \tau_2, \tau_3) = \langle T_\tau[c_i^\dagger(\tau_1)c_j(\tau_2)c_k^\dagger(\tau_3)c_l(0)]\rangle$ is the two-particle Green's function. Here, T_τ is the imaginary time ordering operator and τ_i are imaginary times. The indices i, j, k, l contain the spin and the orbital indices A, B, or C.

To conveniently define the spin and pairing susceptibilities, we define the Fourier transform in the particle-hole (ph) and particle-particle (pp) channels as follows:

$$\chi^{\mathrm{ph},\omega,\omega',\nu}_{ijkl} = \int_0^\beta \int_0^\beta \int_0^\beta d\tau_1 d\tau_2 d\tau_3$$
$$\times \chi_{ijkl}(\tau_1, \tau_2, \tau_3)e^{-i\omega\tau_1}e^{i(\nu+\omega)\tau_2}e^{-i(\nu+\omega')\tau_3}, \quad (7)$$

$$\chi^{\mathrm{pp},\omega,\omega',\nu}_{ijkl} = \int_0^\beta \int_0^\beta \int_0^\beta d\tau_1 d\tau_2 d\tau_3$$
$$\times \chi_{ijkl}(\tau_1, \tau_2, \tau_3)e^{-i\omega\tau_1}e^{i(\nu-\omega')\tau_2}e^{-i(\nu-\omega)\tau_3}, \quad (8)$$

where ν is a bosonic Matsubara frequency and ω and ω' are fermionic Matsubara frequencies.

The generalized susceptibilities can be computed with the impurity solver for the cluster. However, within DMFT, the local cluster susceptibilities are not equal to the lattice susceptibilities. Instead, the self-consistency is only at the level of the local irreducible vertex function Γ, which is the two-particle equivalent to the self-energy. Like the self-energy, Γ is assumed to be momentum independent. It is related to the generalized susceptibilities by the Bethe-Salpeter equation

$$\chi^{\mathrm{c},\omega,\omega',\nu}_{ijkl} = \chi^{\mathrm{c},\omega,\omega',\nu}_{0,ijkl} + \chi^{\mathrm{c},\omega,\omega'',\nu}_{0,ij'ji'}\Gamma^{\mathrm{c},\omega'',\omega''',\nu}_{i'j'k'l'}\chi^{\mathrm{c},\omega''',\omega',\nu}_{k'kl'l}. \quad (9)$$

Here, c denotes the channel and χ_0^c is the bare susceptibility. Repeated indices are summed over. The Bethe-Salpeter equation can be written separately for the cluster and the lattice quantities. The irreducible vertex in each channel is obtained by inverting the Bethe-Salpeter equation for the cluster. The lattice susceptibilities can then be computed by plugging the result in the Bethe-Salpeter equation for the lattice quantities.

We first study the local contributions to the static spin susceptibility, given by

$$\chi^{\mathrm{spin}}_\alpha = \frac{2}{\beta^2}\sum_{\omega,\omega'}\left(\chi^{\mathrm{ph},\omega,\omega',\nu=0}_{\uparrow\alpha,\uparrow\alpha,\uparrow\alpha,\uparrow\alpha} - \chi^{\mathrm{ph},\omega,\omega',\nu=0}_{\uparrow\alpha,\uparrow\alpha,\downarrow\alpha,\downarrow\alpha}\right). \quad (10)$$

These susceptibilities are shown in Fig. 2(a) at half-filling $\mu = 0$. The susceptibility at the B site increases monotonously when the temperature is lowered. This is consistent with Fermi liquid (FL) behavior. On the A/C sites at both $U = -1$ and $U = -2$, the spin susceptibility increases down to $T \approx 0.2|U|$, and then decreases rapidly. This indicates the formation of a pseudogap at the A/C sites. We find this pseudogap also away from the FB, as discussed in [42].

To get further information about the nature of the normal state, we study the Green's functions in the middle of the imaginary time interval, $G_{\alpha\alpha}(\beta/2)$. This quantity is related to the orbital-resolved local spectral function $\mathcal{A}_\alpha$ by [44,45]

$$\beta G_{\alpha\alpha}(\beta/2) = \int \frac{d\omega}{2\pi T}\frac{\mathcal{A}_\alpha(\omega)}{\cosh[\omega/(2T)]}. \quad (11)$$

Since the integral is dominated by the range $\omega \lesssim T$, $\beta G_{\alpha\alpha}(\beta/2)$ approximates $\mathcal{A}_\alpha(\omega = 0)$ at low temperatures. The advantage of studying $\beta G_{\alpha\alpha}(\beta/2)$ is avoiding the analytical continuation necessary to obtain the spectral function within DMFT. However, $\beta G_{\alpha\alpha}(\beta/2)$ is only a reasonable approximation for the spectral function at low temperatures. At half-filling and intermediate interactions, the critical temperature for superconductivity is too high to accurately
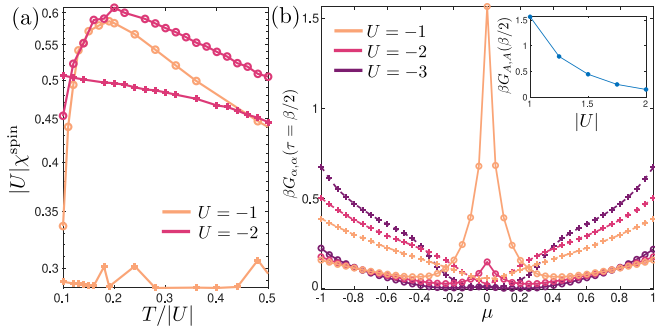
FIG. 2. (a) Orbital-resolved spin susceptibilities $\chi_\alpha^{\text{spin}}$ as a function of $T/|U|$ at half-filling for interaction strengths $U = -1$ and $U = -2$. The susceptibilities are multiplied by the interaction strength for visual clarity. In both (a) and (b), results for the A site are plotted with circles and results for the B site with crosses. The fluctuating data on the B site at $U = -1$ is due to numerical noise in the two-body Green's function. (b) The Green's function $\beta G_{\alpha,\alpha}(\beta/2)$ at inverse temperature $\beta = 20$ as a function of chemical potential. Superconductivity is suppressed. The inset shows $\beta G_{A,A}(\beta/2)$ at half-filling as a function of $|U|$. The results for the A and C sites are identical due to the symmetry of the Lieb lattice.

estimate the spectral function in the normal state using this method. We thus suppress the superconducting order and study $\beta G_{\alpha\alpha}(\beta/2)$ at a low temperature $T = 1/20$. This provides us qualitative information about the nature of the state provided the spectral function does not vary drastically with temperature.

In a FL at zero temperature, the spectral function becomes $\mathcal{A}_\alpha = \rho_\alpha[\mu - \text{Re}\Sigma(\omega = 0)]$, where ρ_α is the orbital-resolved noninteracting density of states. In the Lieb lattice, $\rho_{A/C}$ is infinite at $\mu = 0$ due to the FB. As can be seen from Fig. 2(b), for low interaction strengths, a peak in $\beta G_{AA}(\beta/2)$ is visible. However, when the interaction is increased, $\beta G_{AA}(\beta/2)$ becomes depleted in an increasingly wide region. This confirms the non-Fermi liquid (NFL) behavior in the spin susceptibility at the A/C in Fig. 2(a) is indeed related to a pseudogap in the normal state.

While the spectral function tells about a pseudogap, at low interactions, the imaginary part of the self-energy is helpful in characterizing the FB normal state. In a FL, $\text{Im}\Sigma(i\omega_n)$ vanishes linearly at low frequencies, $\Sigma(i\omega_n) \approx i\omega_n a + b$. As shown in Fig. 3(a), this is observed at the B site. At a low interaction $U = -1$, $\text{Im}\Sigma_{A/C}(\omega)$ instead seems to diverge at $\omega = 0$. As the interaction strength is increased, the divergence disappears and the linear behavior expected for a FL is recovered around $U \approx -1.75$. The imaginary part of the self-energy is related to the quasiparticle weight Z by

$$Z = \left(1 - \frac{\text{Im}\Sigma(i\omega_n)}{\omega_n}\bigg|_{\omega_n \to 0}\right)^{-1}. \qquad (12)$$

Due to the momentum independence of the self-energy within DMFT, $Z = m/m^*$, where m is the bare mass and m^* is the effective mass [46]. The divergence of $\text{Im}\Sigma(i\omega_n)$ around $\omega = 0$ thus indicates a divergence of the effective mass. Therefore, at low interaction strengths, the divergence in the self-energy indicates insulating behavior.
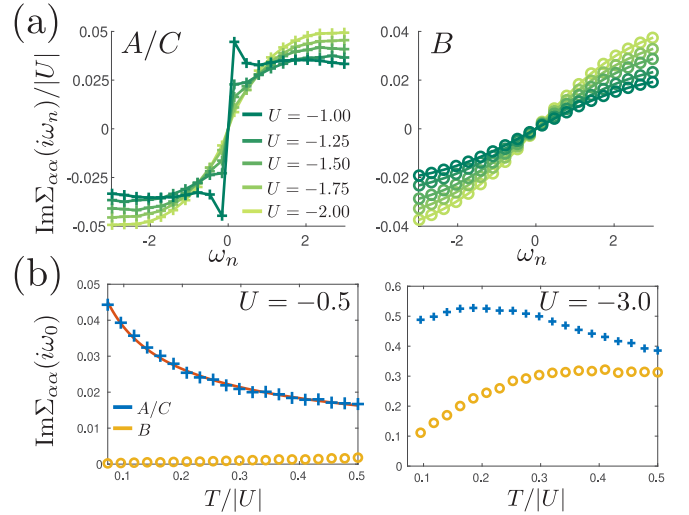

FIG. 3. (a) Imaginary part of the self-energy at half-filling and inverse temperature $\beta = 20$. The superconducting order is suppressed. The left panel shows the divergence of the self-energy, a signature of a NFL insulator, at low interactions on the A/C sites. The right panel shows the behavior at the B site, which is the one expected for a FL. (b) Imaginary part of the self-energy at the first Matsubara frequency, $\text{Im}\Sigma_{\alpha\alpha}(\omega_0 = \pi T)$ as a function of $T/|U|$ at interactions $U = -0.5$ (left) and $U = -3$ (right). The superconducting transition takes place at approximately $T_C \approx 0.06|U|$. In the left panel, the red line shows a power-law fit $(7.9 \times 10^{-3})T^{-0.52}$ to $\text{Im}\Sigma_{AA}(\omega_0)$. On the A/C sites, $\text{Im}\Sigma(\omega_0)$ diverges as the temperature is lowered at $U = -0.5$, whereas it decreases at $U = -3$.

The results presented in Fig. 3(a) are at a low temperature with the superconducting order suppressed. This is necessary because, at high temperatures, the linear vanishing of the self-energy can become invisible if the lowest Matsubara frequency is too high. To verify that the NFL behavior at low interaction strengths exists also when the superconducting transition is not suppressed, we show $\text{Im}\Sigma(i\omega_{n=0})$ as a function of temperature in Fig. 3(b). At $U = -0.5$, $\text{Im}\Sigma(i\omega_{n=0})$ approximately follows a power law proportional to $T^{-1/2}$ (different from, e.g., the Mott insulator T^{-1}), and diverges at low temperature. At $U = -3$, $\Sigma(i\omega_{n=0})$ instead decreases when the critical temperature is approached. This shows the qualitative difference in the behavior of the self-energy at different interaction strengths subsists also when the superconducting order is not suppressed.

DMFT does not allow us to completely discard the possibility of a non-Fermi liquid instead of an insulator. To further study this phase, we use exact diagonalization at zero temperature. The Drude weight [42], shown in Fig. 4(a), decreases with interaction below $|U| \sim 3$. Due to the finite size of the system studied with exact diagonalization, it does not reach zero in the noninteracting case, but it is expected to converge to zero as the bulk limit is approached, meaning the half-filled noninteracting system becomes an insulator. We found a qualitatively similar behavior for the flat band in the kagome lattice [42].

At zero temperature, the insulator cannot subsist at finite interactions. However, at low interactions, transport can be expected to be dominated by pairs, as single particles
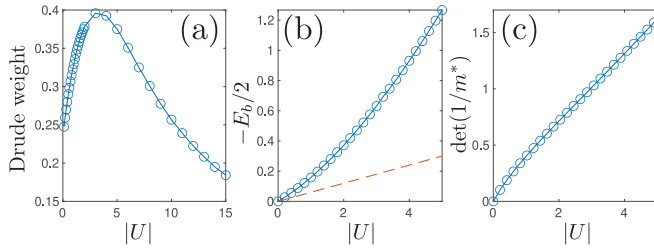
FIG. 4. (a) Drude weight and (b) $-E_b/2$ in the Lieb lattice computed using exact diagonalization at zero temperature and half-filling for a 12-site cluster with periodic boundary conditions. The dashed line in (b) indicates $T_c \approx 0.06|U|$ estimated from the DMFT calculations. (c) Determinant of the inverse effective mass tensor $(1/m^*)$ of two particles on the flat band obtained by solving the two-body problem in the Lieb lattice.

become localized. Thus, we investigate the binding energy of two electrons $E_b = E[(N+1)\uparrow, (N+1)\downarrow] + E(N\uparrow, N\downarrow) - 2E[(N+1)\uparrow, N\downarrow]$, where $E(N\uparrow, M\downarrow)$ is the ground state energy when there are N particles with spin up and M particles with spin down. As can be seen from Fig. 4(b), when the interaction is decreased, the energy per particle needed to break a pair, $-E_b/2$, approaches the critical temperature. At low interaction strengths, the pairs are thus broken by thermal fluctuations already near the superconducting transition. Moreover, the effective mass of a pair in a flat band diverges when the interaction is decreased [1,15], as is seen from the effective mass of two particles on the Lieb lattice flat band shown in Fig. 4(c). An insulator at finite interactions and finite temperature can thus be explained by the diverging effective mass of pairs and their destruction near the superconducting transition, while single particles are localized.

We thus find two different NFL phases in the normal state. When the hopping amplitude is of the order of the interaction or larger, the self-energy at the A/C sites diverges, indicating insulating behavior related to the FB. When the interaction is increased, the insulating behavior disappears as shown by Fig. 3(a), and the spectral function is increasingly suppressed at low temperatures [Fig. 2(a)]. This is a pseudogap phase. The spin susceptibility [Fig. 2(a)] shows NFL features suggesting pairs form already in the normal state also at low interaction strengths. However, the onset temperature of the pseudogap becomes vanishingly close to the superconducting critical temperature at low interaction strengths. In both the insulator and pseudogap cases, the NFL around half-filling is linked to the FB, and the behavior at the B site is that of a FL. We considered weak and intermediate coupling. In the strong-coupling limit, the normal state is expected to contain bosonic pairs as the Bose-Einstein condensation (BEC) limit of the BCS-BEC crossover is reached [16,47,48].

A pseudogap was also predicted in the normal state of the Lieb lattice in [16]. In this Monte Carlo study, a metallic state is predicted at low interaction strengths and a pseudogap phase with short-range pairing correlations at intermediate interactions. In contrast, our results show that the state at low interaction strengths at the FB singularity is not a metallic FL phase. In agreement with this previous study, we find that the normal state at interactions above $|U| \approx 1$ is a pseudogap phase, characterized here by a depletion of the spectral
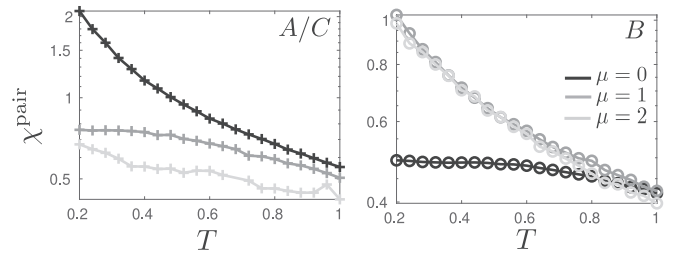

FIG. 5. Pairing susceptibilities $\chi_\alpha^{\mathrm{pair}}$ as a function of temperature for different chemical potentials at interaction strength $U = -2$.

function and a suppressed spin susceptibility. A similar pseudogap state was predicted in [17,18] for lattices with a (quasi) flat band. The onset temperature of the pseudogap in these studies is predicted to be proportional to the interaction strength, which is similar to our result. In summary, we have confirmed by DMFT the presence of a pseudogap in the Lieb lattice, predicted with Monte Carlo studies in flat-band systems. The NFL with insulating behavior we find at low interactions has not been predicted before, and is unique to flat-band systems: it arises from the localization of particles due to destructive quantum interference.

The superconducting phase transition is characterized by the pairing susceptibility, which has local contributions

$$\chi_\alpha^{\mathrm{pair}} = \frac{2}{\beta^2} \sum_{\omega,\omega'} \chi_{\uparrow\alpha,\uparrow\alpha,\downarrow\alpha,\downarrow\alpha}^{\mathrm{pp},\omega,\omega',\nu=0}. \quad (13)$$

The pairing susceptibilities at $U = -2$ and different chemical potentials are shown in Fig. 5(a). At half-filling, the pairing susceptibility is strongly dominated by the A/C sites, where the FB states reside. In contrast, the pairing susceptibility χ_B^{pair} barely increases below $T \approx 0.6$. The total pairing susceptibility diverges at the critical temperature, so this shows that the phase transition is driven by pairing at the A/C sites. When the chemical potential is tuned away from the FB, the susceptibility at the B site becomes the dominant susceptibility. The difference between the susceptibilities in the different sublattices is, however, not as pronounced as at the FB. Even accounting for the different critical temperatures, the pairing susceptibility at the FB singularity is always larger than the local pairing susceptibilities away from the FB. The large difference between the susceptibilities at the A/C and B sites at $\mu = 0$ is thus not only due to a suppression of the susceptibility at the B site, but the FB enhances the local pairing susceptibility at the A/C sites. We have verified that the charge density wave instability, which can compete with the superconducting order in the Lieb lattice at fillings $n = 1/3$ and $n = 2/3$ [47], is weaker than the superconducting instability at $\mu = 1$ and $\mu = 2$ [42].

In summary, we found a crossover between two non-Fermi liquid normal states in the Lieb lattice: a state with insulating characteristics at the A/C sites below interactions of $|U| \simeq 1$ and a metallic state featuring a pseudogap above. The insulator and pseudogap behaviors can coexist in a small temperature range. The crossover can be observed in present-day ultracold gas setups since cooling below T_c, often an obstacle, is not needed, and susceptibilities [49] and pseudogaps [50,51] can be measured. In twisted bilayer graphene (TBG)

the interaction strength is not known, but mean-field studies indicate it is in the regime where flat-band effects are significant [5,52–54]. Thus the possibility of a flat-band insulator interacting normal state should be considered in addition to pseudogap [55] and other exotic normal states [56,57] already observed, in particular for other moiré materials with stronger flat-band character than TBG. Due to the particle-hole symmetry, our results are also relevant for flat-band magnetism [58–60]: the spin susceptibility maps to the charge susceptibility and vice versa.

Pseudogap phases have been predicted and observed in many strongly interacting dispersive systems [21,51,61,62]. For instance, in the square lattice with attractive interactions it appears for large interactions while the weak interaction regime is a Fermi liquid [21]. Here we showed that a flat band enhances the pseudogap formation. The non-Fermi liquid with insulator behavior found at small interactions is qualitatively unique to flat bands.

[1] S. Peotta and P. Törmä, Nat. Commun. **6**, 8944 (2015).

[2] A. Julku, S. Peotta, T. I. Vanhala, D.-H. Kim, and P. Törmä, Phys. Rev. Lett. **117**, 045303 (2016).

[3] L. Liang, T. I. Vanhala, S. Peotta, T. Siro, A. Harju, and P. Törmä, Phys. Rev. B **95**, 024515 (2017).

[4] T. Hazra, N. Verma, and M. Randeria, Phys. Rev. X **9**, 031049 (2019).

[5] F. Xie, Z. Song, B. Lian, and B. A. Bernevig, Phys. Rev. Lett. **124**, 167002 (2020).

[6] V. A. Khodel and V. R. Shaginyan, Pis'ma Zh. Eksp. Teor. Fiz. **51**, 488 (1990) [JETP Lett. **51**, 553 (1990)].

[7] V. Khodel, V. Shaginyan, and V. Khodel, Phys. Rep. **249**, 1 (1994).

[8] T. T. Heikkilä, N. B. Kopnin, and G. E. Volovik, JETP Lett. **94**, 233 (2011).

[9] N. B. Kopnin, T. T. Heikkilä, and G. E. Volovik, Phys. Rev. B **83**, 220503(R) (2011).

[10] Y. Cao, V. Fatemi, A. Demir, S. Fang, S. L. Tomarken, J. Y. Luo, J. D, Sanchez-Yamagishi, K. Watanabe, T. Taniguchi, E. Kaxiras, R. C. Ashoori, and P. Jarillo-Herrero, Nature (London) **556**, 80 (2018).

[11] Y. Cao, V. Fatemi, S. Fang, K. Watanabe, T. Taniguchi, E. Kaxiras, and P. Jarillo-Herrero, Nature (London) **556**, 43 (2018).

[12] M. Yankowitz, S. Chen, H. Polshyn, Y. Zhang, K. Watanabe, T. Taniguchi, D. Graf, A. F. Young, and C. R. Dean, Science **363**, 1059 (2019).

[13] P. Gurin and Z. Gulácsi, Phys. Rev. B **64**, 045118 (2001).

[14] M. Tovmasyan, S. Peotta, L. Liang, P. Törmä, and S. D. Huber, Phys. Rev. B **98**, 134513 (2018).

[15] P. Törmä, L. Liang, and S. Peotta, Phys. Rev. B **98**, 220511(R) (2018).

[16] N. Swain and M. Karmakar, Phys. Rev. Research **2**, 023136 (2020).

[17] J. S. Hofmann, E. Berg, and D. Chowdhury, Phys. Rev. B **102**, 201112(R) (2020).

[18] V. Peri, Z.-D. Song, B. A. Bernevig, and S. D. Huber, Phys. Rev. Lett. **126**, 027002 (2021).

[19] T. A. Maier, M. Jarrell, T. Prushke, and M. Hettler, Rev. Mod. Phys. **77**, 1027 (2005).

[20] M. Capone, C. Castellani, and M. Grilli, Phys. Rev. Lett. **88**, 126403 (2002).

[21] M. Keller, W. Metzner, and U. Schollwöck, Phys. Rev. Lett. **86**, 4612 (2001).

[22] A. Toschi, P. Barone, M. Capone, and C. Castellani, New J. Phys. **7**, 7 (2005).

[23] R. Peters and J. Bauer, Phys. Rev. B **92**, 014511 (2015).

[24] X. Chen, J. P. F. LeBlanc, and E. Gull, Phys. Rev. Lett. **115**, 116402 (2015).

[25] H. Shinaoka, S. Hoshino, M. Troyer, and P. Werner, Phys. Rev. Lett. **115**, 156401 (2015).

[26] P. Kumar, T. I. Vanhala, and P. Törmä, Phys. Rev. B **100**, 125141 (2019).

[27] P. Kumar, S. Peotta, Y. Takasu, Y. Takahashi, and P. Törmä, Phys. Rev. A **103**, L031301 (2021).

[28] E. W. Huang, M.-S. Vaezi, Z. Nussinov, and A. Vaezi, Phys. Rev. B **99**, 235128 (2019).

[29] S. Sayyad, E. W. Huang, M. Kitatani, M.-S. Vaezi, Z. Nussinov, A. Vaezi, and H. Aoki, Phys. Rev. B **101**, 014501 (2020).

[30] S. Taie, H. Ozawa, T. Ichinose, T. Nishio, S. Nakajima, and Y. Takahashi, Sci. Adv. **1**, e1500854 (2015).

[31] H. Ozawa, S. Taie, T. Ichinose, and Y. Takahashi, Phys. Rev. Lett. **118**, 175301 (2017).

[32] M. R. Slot, T. S. Gardenier, P. H. Jacobse, G. C. P. van Miert, S. N. Kempkes, S. J. M. Zevenhuizen, C. M. Smith, D. Vanmaekelbergh, and I. Swart, Nat. Phys. **13**, 672 (2017).

[33] R. Drost, T. Ojanen, A. Harju, and P. Liljeroth, Nat. Phys. **13**, 668 (2017).

[34] S. Mukherjee, A. Spracklen, D. Choudhury, N. Goldman, P. Öhberg, E. Andersson, and R. R. Thomson, Phys. Rev. Lett. **114**, 245504 (2015).

[35] B. Cui, X. Zheng, J. Wang, D. Liu, S. Xie, and B. Huang, Nat. Commun. **11**, 66 (2020).

[36] L. Balents, C. R. Dean, D. K. Efetov, and A. F. Young, Nat. Phys. **16**, 725 (2020).

[37] T. I. Vanhala, T. Siro, L. Liang, M. Troyer, A. Harju, and P. Törmä, Phys. Rev. Lett. **116**, 225305 (2016).

[38] I. S. Tupitsyn and N. V. Prokof'ev, Phys. Rev. B **99**, 121113(R) (2019).

[39] M. Tovmasyan, S. Peotta, P. Törmä, and S. D. Huber, Phys. Rev. B **94**, 245149 (2016).

[40] F. F. Assaad and T. C. Lang, Phys. Rev. B **76**, 035116 (2007).

[41] E. Gull, A. J. Millis, A. I. Lichtenstein, A. N. Rubtsov, M. Troyer, and P. Werner, Rev. Mod. Phys. **83**, 349 (2011).

[42] See Supplemental Material at http://link.aps.org/supplemental/10.1103/PhysRevB.103.L220502 for details on the method to compute generalized susceptibilities, discussion of pseudogap behavior away from the flat-band, results for the charge susceptibility, details on the computation of the Drude weight using exact diagonalization, and exact diagonalization results in the kagome lattice, which includes Refs. [63,64].

[43] G. Rohringer, A. Valli, and A. Toschi, Phys. Rev. B **86**, 125114 (2012).

[44] E. Gull, O. Parcollet, P. Werner, and A. J. Millis, Phys. Rev. B **80**, 245102 (2009).

[45] N. Trivedi and M. Randeria, Phys. Rev. Lett. **75**, 312 (1995).

[46] E. Müller-Hartmann, Int. J. Mod. Phys. B **03**, 2169 (1989).

[47] V. I. Iglovikov, F. Hébert, B. Grémaud, G. G. Batrouni, and R. T. Scalettar, Phys. Rev. B **90**, 094506 (2014).

[48] *The BCS-BEC Crossover and the Unitary Fermi Gas*, edited by W. Zwerger, Lecture Notes in Physics Vol. 836 (Springer, Heidelberg, 2012).

[49] J. Meineke, J.-P. Brantut, D. Stadler, T. Müller, H. Moritz, and T. Esslinger, Nat. Phys. **8**, 454 (2012).

[50] J. P. Gaebler, J. T. Stewart, T. E. Drake, D. S. Jin, A. Perali, P. Pieri, and G. C. Strinati, Nat. Phys. **6**, 569 (2010).

[51] M. Feld, B. Fröhlich, E. Vogt, M. Koschorreck, and M. Köhl, Nature (London) **480**, 75 (2011).

[52] A. Julku, T. J. Peltonen, L. Liang, T. T. Heikkilä, and P. Törmä, Phys. Rev. B **101**, 060505(R) (2020).

[53] X. Hu, T. Hyart, D. I. Pikulin, and E. Rossi, Phys. Rev. Lett. **123**, 237002 (2019).

[54] L. Classen, Physics **13**, 23 (2020).

[55] Y. Jiang, X. Lai, K. Watanabe, T. Taniguchi, K. Haule, J. Mao, and E. Y. Andrei, Nature (London) **573**, 91 (2019).

[56] U. Zondiner, A. Rozen, D. Rodan-Legrain, Y. Cao, R. Queiroz, T. Taniguchi, K. Watanabe, Y. Oreg, F. von Oppen, A. Stern, E. Berg, P. Jarillo-Herrero, and S. Ilani, Nature (London) **582**, 203 (2020).

[57] D. Wong, K. P. Nuckolls, M. Oh, B. Lian, Y. Xie, S. Jeon, K. Watanabe, T. Taniguchi, B. A. Bernevig, and A. Yazdani, Nature (London) **582**, 198 (2020).

[58] A. Mielke, J. Phys. A: Math. Gen. **25**, 4335 (1992).

[59] H. Tasaki, Phys. Rev. Lett. **69**, 1608 (1992).

[60] A. Mielke and H. Tasaki, Commun. Math. Phys. **158**, 341 (1993).

[61] C. Huscroft, M. Jarrell, T. Maier, S. Moukouri, and A. N. Tahvildarzadeh, Phys. Rev. Lett. **86**, 139 (2001).

[62] E. Gull, O. Parcollet, and A. J. Millis, Phys. Rev. Lett. **110**, 216405 (2013).

[63] T. Siro and A. Harju, Comput. Phys. Commun. **183**, 1884 (2012).

[64] E. Dagotto, Rev. Mod. Phys. **66**, 763 (1994).